Journal of Reliability
Science and
Engineering

PAPER • OPEN ACCESS

Topology and reliability-based design optimization for dual rotary tables of five-axis CNC machine tools

To cite this article: Dongheng Li *et al* 2025 *J. Reliab. Sci. Eng.* **1** 045401

View the article online for updates and enhancements.

You may also like

- Adaptive artificial neural network for uncertainty propagation
Yan Shi, Lizhi Niu and Michael Beer
- Time-variant system reliability analysis via stochastic process discretization and most probable point trajectory approximation
Dequan Zhang, Hongfei Zhang, Pengfei Zhou et al.
- Probabilistic calibration of model parameters with approximate Bayesian quadrature and active machine learning
Pengfei Wei, Masaru Kitahara, Matthias G R Faes et al.

This content was downloaded from IP address 118.123.172.215 on 11/11/2025 at 04:16

OPEN ACCESS
IOP Publishing | ISECAEP
Journal of Reliability Science and Engineering
J. Reliab. Sci. Eng. **1** (2025) 045401 (13pp)
https://doi.org/10.1088/3050-2454/ae179a

Topology and reliability-based design optimization for dual rotary tables of five-axis CNC machine tools

Dongheng Li[1], Mingfei Ma[1], Xianzhen Huang[1,2,*], Yuping Wang[1], Zhiyuan Lu[1] and Peilong Li[1]

[1] School of Mechanical Engineering and Automation, Northeastern University, Shenyang, 110819, People's Republic of China
[2] Laboratory of Vibration and Control of Aero-Propulsion Systems Ministry of Education of China, Northeastern University, 110819 Shenyang, People's Republic of China

E-mail: 236126114@qq.com

Received 27 June 2025, revised 27 September 2025
Accepted for publication 26 October 2025
Published 5 November 2025

Abstract

This paper proposes a design optimization scheme for the dual rotary table of a five-axis CNC machine tool. In the preliminary structural design, topology optimization is employed to eliminate restrictions on configurations caused by subjective factors such as empirical knowledge. Accounting for stochastic uncertainties, reliability-based design optimization is implemented on the topology-optimized structure. The reliability index is computed via Monte Carlo simulation (MCS), while the optimal structural solution is iteratively derived using a whale optimization algorithm integrated with adaptive kriging for MCS. The effectiveness of the optimized solution is ultimately validated through case studies.

Keywords: five-axis CNC machine tool, topology optimization, reliability-based design optimization, kriging

1. Introduction

Five-axis CNC machine tools are core equipment for precision machining of complex components in critical sectors like precision instrumentation, aerospace, and automotive industries [1–4]. The machining accuracy they achieve reflects a nation's industrial advancement level. Featuring superior stability and unparalleled precision, dual rotary tables (*A* and *C* axes) have become the preferred solution for modern five-axis machine worktables [5–8]. Within dual rotary table systems, the cradle frame forms the structural skeleton, bearing combined gravitational and machining loads while handling positioning and motion control tasks. Lightweighting this component significantly reduces drive system burden, resulting in improved positioning accuracy and enhanced dynamic response [9–11]. An integrated design utilizing thin-wall shells with strategically placed stiffeners achieves substantial mass reduction without compromising structural rigidity or robustness [12–14]. However, conventional stiffener design relies on empirical knowledge, trapping engineers in inefficient loops of 'design-prototype-test' iterations [15–17].

Recent advances in computing power have positioned topology optimization as a widely adopted method for machine tool component design among global researchers. This approach enables unrestricted material redistribution within the design domain, liberating structural

* Author to whom any correspondence should be addressed.

Original content from this work may be used under the terms of the Creative Commons Attribution 4.0 licence. Any further distribution of this work must maintain attribution to the author(s) and the title of the work, journal citation and DOI.

© 2025 The Author(s). Published by IOP Publishing Ltd on behalf of the Institute of Systems Engineering, China Academy of Engineering Physics

configurations from empirical biases and other subjective constraints.

Yoshimura and Izui [18] pioneered a hierarchical representation of machine tool structures through genotype encoding, capturing system-component-part relationships, and conducted topology optimization via genetic algorithms (GAs). Cui *et al* [19] developed a polygonal topology optimization framework incorporating an alternating active-phase algorithm for multi-material systems, eliminating sensitivity filtering requirements while resolving geometric complexities and suppressing numerical instabilities. Liu *et al* [20] established a ground structure method -driven stiffener layout optimization, applying topology optimization to spindle box covers with thickness penalization that significantly enhanced fundamental frequencies. Veluswamy *et al* [21] achieved concurrent mass reduction and dynamic property enhancement in vertical machining center columns through topology optimization, ultimately reducing workpiece surface roughness.

However, current topology optimization faces significant limitations when applied to large-scale complex-curvature components, frequently manifesting structural homogenization and irrational material deposition that compromise solution validity. Hao *et al* [22] leveraged parallels between natural leaf vein patterns and machine tool rib layouts to develop a variable-cross-section optimization method for support structures. Audibert *et al* [23] developed a bone-inspired structural optimization methodology that employs stress-dependent porosity distribution to achieve lightweight designs with mechanical performance comparable to conventional topology optimization, validated through experimental testing demonstrating reduced workpiece mass while preserving structural resistance. Nevertheless, bio-inspired structural optimization remains constrained by incomplete theoretical frameworks and limited mature biological prototypes, rendering such outcomes primarily suitable as preliminary configuration references.

Since Yeh and Vance [24] pioneered the integration of size sensitivity analysis into finite element modeling, sensitivity-based optimization methods have evolved into core methodologies in structural optimization, valued for their solution clarity and computational reliability. Shan *et al* [25] implemented an automated structural optimization framework for multilateral force-resisting systems by combining enhanced sensitivity analysis and a modified Hooke–Jeeves algorithm to minimize material costs while satisfying design code constraints and maintaining structural safety. Ma *et al* [26] proposed and implemented a global reliability sensitivity analysis method based on a Bayesian framework for the dual rotary table. This approach demonstrated significant computational efficiency and provided critical insights for design optimization.

With the continuous advancement of design and manufacturing capabilities in the mechanical industry, merely fulfilling basic functional requirements can no longer meet the escalating performance demands for mechanical products. This context has propelled the emergence and development of reliability-based design optimization (RBDO). Over decades of evolution, RBDO has established a relatively complete theoretical framework and a clear trajectory for technological progress. Recent advancements in RBDO focus on overcoming computational burdens. Meng *et al* [27] proposed a fidelity transformation framework converting high-fidelity RBDO to efficient low-fidelity versions without accuracy loss. Lu *et al* [28] developed an improved kriging method using sample-distribution learning functions and incremental sampling to accelerate constraint modeling and deterministic conversion. Meng *et al* [29] introduced a unified framework featuring parallel reliability computation decoupling and adaptive optimization for complex multimodal problems. Collectively, these works enhance RBDO efficiency through surrogate modeling, transformation strategies, and parallelization.

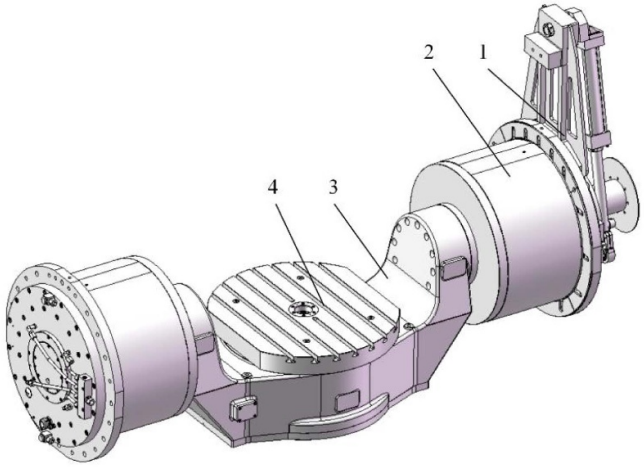
This study proposes a full process design optimization methodology dedicated to the dual rotary table, integrating advanced techniques to drive development from initial conceptual design to finalized structural configuration. The methodology begins with density-based topology optimization, where finite element analysis (FEA) identifies stress concentration zones. Based on this analysis, stiffening ribs are strategically positioned at critical load-bearing locations, significantly enhancing structural static stiffness. Subsequently, the optimized geometry undergoes RBDO through a parametric model. To overcome premature convergence in traditional gradient algorithms, the whale optimization algorithm (WOA) metaheuristic algorithm is introduced, effectively escaping local optima. Within this RBDO framework, Monte Carlo simulation (MCS) quantifies aleatoric uncertainties to ensure structural reliability [30]. The final design achieves synergistic mass reduction and structural robustness enhancement.

2. Structural mechanics analysis

Figure 1 illustrates the mechanical model of the dual rotary table, consisting primarily of the cradle frame, worktable, *C*-axis motor and bearings, *A*-axis motor and bearings, along with braking and counterbalance mechanisms. Serving as the structural backbone of the system, the cradle frame constitutes the optimization target in this study. Structural mechanics analysis of the dual rotary table follows a workflow comprising pre-processing, iterative computation, and post-processing stages, with the complete procedure detailed in figure 2.

2.1. Simplified model

During actual machining operations, structures such as bolts, chamfers, and oil passages in the dual rotary table exert negligible influence on static stiffness. Meanwhile, internal components including motors and bearings constitute standardized parts, rendering structural modifications redundant. Therefore, after comprehensively evaluating actual operating conditions and FEA precision and efficiency requirements, the dual rotary



(1) Braking module (2) A-axis housing (3) Cradle frame (4) Worktable

Figure 1. Structural schematic diagram of the dual rotary table.

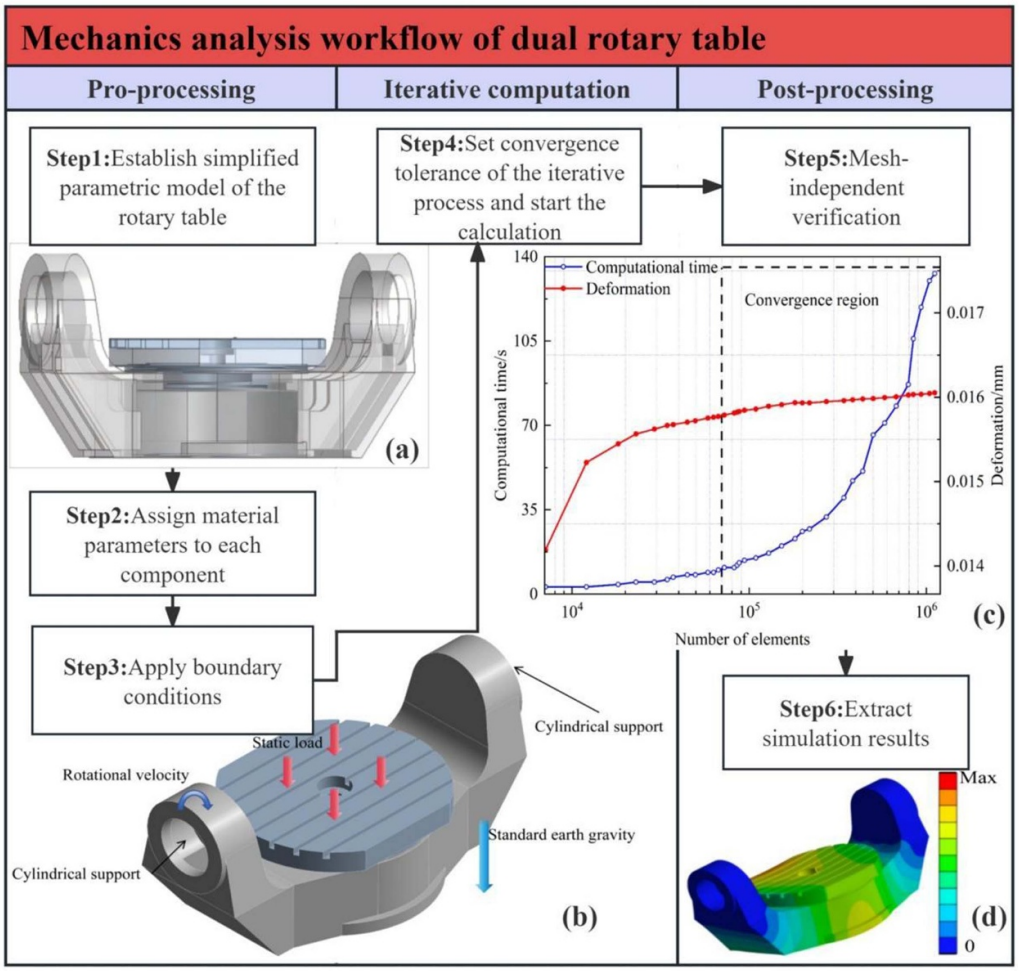
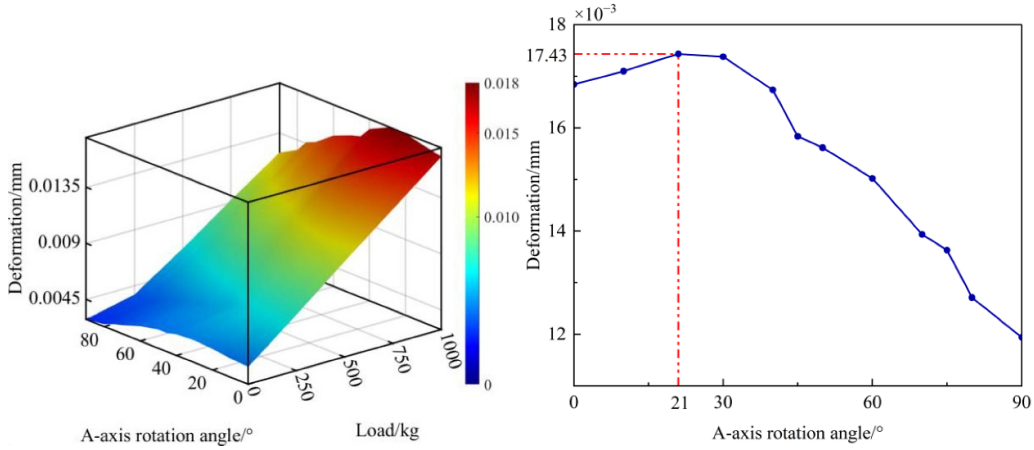


Figure 2. Mechanics analysis flowchart. (a) Deformation nephogram under load and rotation and (b) deformation variation with *A*-axis rotation angle.



(a) Deformation nephogram under load and rotation (b) Deformation variation with A-axis rotation angle

Figure 3. Load-induced deformation analysis of the dual rotary table.

table model was streamlined to its core structural components, as illustrated figure 2(a).

2.2. Boundary conditions

In FEA, sliding contact constraints preventing normal separation were applied at the worktable-cradle frame interface to simulate relative motion with maintained contact. Cylindrical constraints were established at both ends of the cradle frame bearing connections to the braking module. A prescribed rotational velocity of 50 rpm about the *A*-axis was imposed, consistent with product specifications. Static loads were uniformly distributed as pressure on the worktable surface, centered at its geometric origin. The fully constrained finite element model is shown in figure 2(b). Concurrently, material properties were assigned to all components with iterative convergence tolerance set at 0.5%.

2.3. Mesh independence verification

In this study, hexahedral elements were exclusively employed for FEA, leveraging their superior isotropy and convergence characteristics [31]. Mesh independence verification is essential for ensuring the accuracy and efficiency of FEA. For the finite element model, this verification spanned an element count range of 7×10^3–1.1×10^6, with results presented in figure 2(c). Under consistent boundary conditions, material properties, and loading configurations, the mesh was incrementally refined while monitoring variations in computed deformation magnitudes. Convergence was achieved when solution differences between successive refinements stabilized below 0.15%, establishing the tolerance threshold for grid-induced influence. This criterion defined the converged region shown in figure 2(c).

2.4. Mechanical results analysis

Following the aforementioned procedures, FEA was performed via ANSYS Mechanical (v2023 R1) using hexahedral elements with a uniform size of 15 mm. Figure 3 displays the variation in system deformation under different *A*-axis rotation angles and worktable loading conditions. Maximum deformation of 0.017 432 mm occurred at the critical operating state with 21° *A*-axis rotation under the rated maximum load. Structural design and optimization were subsequently performed under this limiting condition to validate the superiority of the proposed topology and RBDO framework for dual rotary tables.

3. Topology optimization

Topology optimization achieves specified performance targets (e.g. peak stiffness, natural frequencies) by redistributing material within a prescribed design domain. Compared to traditional size and shape optimization, it transcends initial design constraints through free material distribution, generating optimal structural configurations that satisfy performance criteria. However, practical applications face multidimensional limitations, including prohibitive computational costs for high-resolution complex models and susceptibility to multiaxial failure modes under singular objectives. This study adopts a two-stage topology optimization methodology, transforming the dual rotary table from conceptual design to a validated baseline structure.

3.1. Density-based topology optimization

The density-based method represents the most widely adopted topology optimization approach, fundamentally transforming material distribution in continuous media into a discretized density-field optimization model. Using element relative densities as design variables, this method establishes functional relationships between density and material elastic modulus (i.e. pseudo-density) to intuitively characterize material retention or removal. By incorporating the solid isotropic material with penalization (SIMP) density-stiffness interpolation model, intermediate densities are penalized through penalty

exponents, driving material distributions toward binary 0/1 convergence throughout iterations [32].

3.2. Topology optimization formulation

The two-stage topology optimization methodology is executed sequentially with distinct objectives: the global stage performs topology optimization of the entire dual rotary table for mass minimization, while the local stage conducts topology optimization of stress concentration zones for compliance minimization, addressing distinct objectives and optimization targets at each phase. The global topology optimization in this study aims to minimize mass while constrained by nodal displacements and symmetry about the *YZ*-plane. This optimization problem is formulated as:

$$\begin{aligned} &\min\ M(\boldsymbol{\rho}) = \sum_{i=1}^{N} \rho_i v_i \\ &\text{s.t.} \quad \boldsymbol{K}(\boldsymbol{\rho}) = \sum_{i=1}^{N} \rho_i^p \boldsymbol{K}_i \\ &\boldsymbol{K}(\boldsymbol{\rho})\boldsymbol{U} = \boldsymbol{F} \\ &\rho_i = \rho_{is} \\ &0 < \rho_{\min} \leqslant \rho_i \leqslant 1 \end{aligned} \tag{1}$$

where $M(\boldsymbol{\rho})$ represents the total mass of the dual rotary table, N defines the total number of discrete elements, $\boldsymbol{K}(\boldsymbol{\rho})$ denotes the total stiffness matrix of the element. ρ_i is the pseudo-density at element, $\rho_i = 1$ indicates material retention, $\rho_i = \rho_{\min}$ indicates material approximates void, $\rho_i = 0$ indicates material removal, $\rho_{\min}$ prevents stiffness matrix singularity, typically set to 10^{-3}, ν_i is the volume of element *e*, p represents the SIMP penalty exponent with $p \geqslant 3$, $\boldsymbol{K}_i$ is the element stiffness matrix, $\boldsymbol{U}$ represents the elemental displacement vector, $\boldsymbol{F}$ represents the global external load vector, *is* represents the symmetric elemental load for element *i*.

Local topology optimization is performed on the simplified mechanical model to minimize compliance (maximize stiffness) under symmetry constraints. Extrusion constraints are simultaneously imposed to ensure manufacturable structures. Compliance is calculated as:

$$\boldsymbol{C} = \boldsymbol{U}^{\mathrm{T}}\boldsymbol{K}\boldsymbol{U} = \frac{1}{2}\int_{\Omega} \varepsilon^{\mathrm{T}}\boldsymbol{D}\varepsilon \mathrm{d}\Omega \tag{2}$$

where $\boldsymbol{C}$ represents the elemental compliance, $\boldsymbol{U}$ represents the elemental displacement vector, $\boldsymbol{K}$ is the elemental stiffness matrix, Ω is the design domain, ε is the strain tensor, $\boldsymbol{D}$ represents the elasticity matrix.

3.3. Implementation workflow of the two-stage topology optimization

This study conducted a two-stage topology optimization for the dual rotary table system. The initial global stage pursued mass minimization using a geometrically simplified solid model (figure 4(a)) retaining only fundamental features. With operational constraints and loads applied, FEA yielded the preliminary structure in figure 4(b). Given the system's complex geometry and stringent stiffness requirements, standalone global optimization proved insufficient. Subsequent local refinement targeted stress concentration zones identified via FEA (**Zone 1 in** figure 4(c)). The rib region was parametrically modeled as a rectangular domain under bidirectional loading with front and rear supports, undergoing compliance-minimized topology optimization (figure 4(d)). Final verification confirmed a 19.94% deformation reduction after rib implementation, validating enhanced static stiffness. This sequential approach delivered a structurally efficient configuration with balanced mass-stiffness performance.

4. RBDO of structural parameters

4.1. Reliability calculation

While topology optimization yields configurations satisfying mechanical performance requirements, it cannot generate deterministic dimensional parameters. To overcome this limitation, this study employed a hybrid metaheuristic algorithm integrating adaptive kriging ((AK)-MCS) with WOA for iterative solutions, ultimately producing a deterministic optimization (DDO) scheme.

Based on the topology-optimized base structure, ten key dimensional parameters were extracted and served as input variables for the subsequent optimization design,

$$\boldsymbol{X} = [D_i]^{\mathrm{T}} \tag{3}$$

where D_i are dimensional parameters, D_1 designates the stiffening rib inclination angle, D_2 to D_7 specify stiffening rib thicknesses, D_8 defines the stiffening rib web angle, D_9 represents the core tube thickness, and D_{10} denotes the side skirt height.

Under maximum loading conditions, the deformation of the dual rotary table exhibits a nonlinear relationship with *A*-axis rotation angles, while the coupling deformation contribution from worktable rotation about the *C*-axis is statistically negligible. At rated maximum load, maximum deformation occurs at 21° *A*-axis rotation of the cradle frame, defining the system's limit state. This can be mathematically defined as:

$$g(\boldsymbol{X}) = L_{\max} - L(\boldsymbol{X}) \tag{4}$$

$$g^*(\boldsymbol{X}) = L^*_{\max} - L^*(\boldsymbol{X}) \tag{5}$$

where the total deformation of the system is denoted as $L(\boldsymbol{X})$, with its maximum value $L_{\max} = 0.017\,432$ mm at the ultimate state. Axial deformation is specified by $L^*(\boldsymbol{X})$, where the maximum axial deformation $L^*_{\max} = 0.014\,582$ mm (*Y*-direction).

When the limit state function exceeds zero, the dual rotary table operates in a reliable state. Integration over the probability density function of random variables yields the system

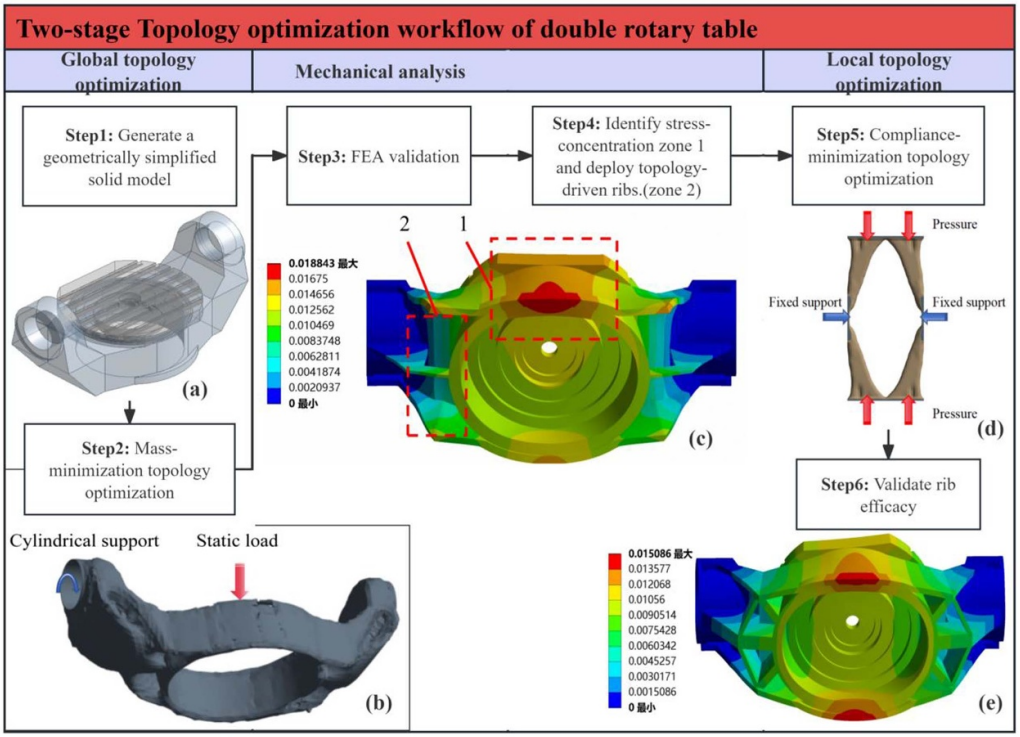


Figure 4. The two-stage topology optimization flowchart.

reliability under the current stiffening rib layout:

$$P_f = \int_{g(\boldsymbol{X})>0 \cap g^*(\boldsymbol{X})>0} f(x_1, x_2, \ldots x_n)\, \mathrm{d}x_1 \mathrm{d}x_2 \ldots \mathrm{d}x_n. \tag{6}$$

The Monte Carlo method is a statistical approach that estimates numerical results through random sampling [33, 34], mathematically expressed as:

$$E[f(\boldsymbol{X})] = \frac{1}{N}\sum_{i=1}^{N} f\left(\boldsymbol{x}^{(i)}\right) \tag{7}$$

where $E[f(\boldsymbol{X})]$ denotes the mathematical expectation of function $f(\boldsymbol{X})$, $\boldsymbol{X}$ is a random variable following distribution $p(x)$, N represents the number of independent samples.

4.2. AK surrogate model construction

While the Monte Carlo method can directly compute reliability, it requires substantial FEA samples, incurring prohibitive time costs. To enhance computational efficiency, the AK surrogate (AKS) model was thus employed. This approach fundamentally fits data samples through spatial interpolation, combining global approximation with local stochastic errors to achieve minimum unbiased variance estimation [35]. For the optimization problem in this study, the mathematical formulation is expressed as:

$$h_{k_n}(\boldsymbol{X}) = \sum_{i=1}^{N} f_i(\boldsymbol{X})\,\boldsymbol{\beta}_i + z(\boldsymbol{X}), n = 1,2 \tag{8}$$

where $h_{k1}(\boldsymbol{X})$ represents the deformation L AKS model and $h_{k2}(\boldsymbol{X})$ represents the mass M AKS model. Each model comprises basis functions $f_i(\boldsymbol{X})$ of random variables $\boldsymbol{X}$, regression coefficients $\boldsymbol{\beta}$ scaling with response estimates, and N denoting the basis function count. The stochastic process $z(\boldsymbol{X})$ has a covariance structure given in equation (9):

$$\mathrm{cov}\left[z\left(\boldsymbol{x}^{(i)}\right), z\left(\boldsymbol{x}^{(j)}\right)\right] = \sigma^2\left[R\left(\boldsymbol{x}^{(i)}, \boldsymbol{x}^{(j)}\right)\right] \tag{9}$$

where $(\boldsymbol{x}^{(i)}, \boldsymbol{x}^{(j)})$ represents the sample points. The correlation function $R(\boldsymbol{X})$ in equation (10) adopts Gaussian form due to its computational efficacy:

$$R\left(\boldsymbol{x}^{(i)}, \boldsymbol{x}^{(j)}\right) = \exp\left(-\sum_{h=1}^{N}\theta\left|\boldsymbol{x}_h^{(i)} - \boldsymbol{x}_h^{(j)}\right|^2\right). \tag{10}$$

The AKS model constructed in this study for deformation L and mass M of the dual rotary table is mathematically expressed as:

$$\begin{aligned} h_{k_n}(\boldsymbol{x}) &= \boldsymbol{f}^{\mathrm{T}}(\boldsymbol{x})\,\hat{\boldsymbol{\mu}} + \boldsymbol{r}^{\mathrm{T}}(\boldsymbol{x})\boldsymbol{R}^{-1}(\boldsymbol{g} - \boldsymbol{A}\hat{\boldsymbol{\mu}}), n = 1,2 \\ \hat{\boldsymbol{\mu}} &= \left(\boldsymbol{A}^{\mathrm{T}}\boldsymbol{R}^{-1}\boldsymbol{A}\right)^{-1}\boldsymbol{A}^{\mathrm{T}}\boldsymbol{R}^{-1}\boldsymbol{g} \\ \hat{\boldsymbol{\sigma}}^2 &= (\boldsymbol{g} - \boldsymbol{A}\boldsymbol{\beta})^{\mathrm{T}}\boldsymbol{R}^{-1}(\boldsymbol{g} - \boldsymbol{A}\boldsymbol{\beta})/m \\ \max F(\boldsymbol{\theta}) &= -\frac{m\ln\left(\hat{\boldsymbol{\sigma}}^2\right) + \ln|\boldsymbol{R}|}{2} \\ U(\boldsymbol{x}) &= \left|\frac{\hat{\boldsymbol{\mu}}}{\hat{\boldsymbol{\sigma}}}\right| \end{aligned} \tag{11}$$

where $\hat{\boldsymbol{\mu}}$ denotes the estimated mean of $\boldsymbol{\mu}$, $\hat{\boldsymbol{\sigma}}^2$ represents the variance estimator of σ^2, g is the column vector of finite element sample response values, A indicates the m $\times$ n basis matrix constructed from finite element regression models, $r(x)$ defines the correlation vector between actual FEA training samples and predicted values, and θ signifies the hyperparameters in the correlation function, determined through the maximization criterion.

The U-learning function incorporates two key dependencies: prediction distance to failure boundary and standard deviation of estimates. Specifically, when predictions are identical, larger standard deviations yield smaller U-values; when standard deviations are identical, predictions closer to zero reduce U-values. Active learning selects sample points that minimize U-values from the candidate pool, prioritizing points with high proximity to the failure boundary and high uncertainty. These points then update the kriging model using corresponding mass and deformation metrics. Based on the convergence criterion defined in [36] and adapted to our experimental conditions, convergence is achieved when 10 consecutive sample sets satisfy min $U(\boldsymbol{x}) \geqslant 2$, with the total sample size reaching 90 at convergence.

This study employs the AKS model incorporating MCS to replace computationally intensive finite element models. With dimensional parameters of samples as independent variables and FEA-calculated deformation as response values, separate AK models were constructed for the deformation L and mass M of the dual rotary table. The analysis workflow is shown in figure 5.

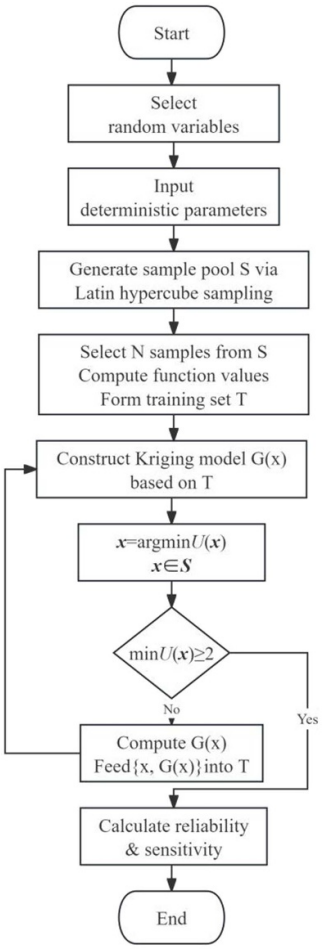


Figure 5. Flowchart of AKS model construction.

4.3. Optimization algorithms

This chapter implements RBDO of structural parameters, with the strategy of minimizing system mass while satisfying stiffness and reliability constraints. The optimization problem is formulated mathematically in equation (12),

$$\begin{aligned} &\min M(\boldsymbol{X}) \\ &\text{s.t.} \quad R_i(\boldsymbol{X}) \leqslant 0 \\ &\qquad G_i(\boldsymbol{X}) \leqslant 0 \\ &\boldsymbol{X}_{\min} \leqslant \boldsymbol{X} \leqslant \boldsymbol{X}_{\max} \end{aligned} \tag{12}$$

where $\boldsymbol{X}$ is the column vector of dimensional parameters, $R_i(\boldsymbol{X})$ denotes reliability constraints, $G_i(\boldsymbol{X})$ represents stiffness constraints; $\boldsymbol{X}_{\min}$ and $\boldsymbol{X}_{\max}$ are the lower and upper bounds of dimensional parameters.

Conventional gradient-based optimization methods typically converge to local optima, failing to achieve global solutions. To overcome this limitation in RBDO, this study employs a metaheuristic algorithm framework. To eliminate stochastic bias in performance evaluation, five independent trials were conducted for WOA, GA, Salp Swarm Algorithm, and Red Fox optimization. Figure 6 displays representative convergence curves from a single trial, demonstrating WOA's superior convergence rate. WOA escapes local optima by simulating humpback whales' bubble-net hunting behavior. This exceptional performance stems from WOA's unique spiral bubble-net attacking mechanism, which achieves superior dynamic balance between exploration and exploitation, enhancing global search capability and accelerating convergence. Consequently, WOA was selected as the core solver for RBDO problems to ensure high-quality optimal solutions.

WOA achieves global optima by simulating humpback whale foraging behavior through spiral movements [37–39]. Its mathematical formulation is expressed as:

$$\begin{aligned} \boldsymbol{P}(\boldsymbol{t}+1) &= \begin{cases} \boldsymbol{P}^*(\boldsymbol{t}) - \boldsymbol{QT}, & p < 0.5 \cap |\boldsymbol{Q}| < 1 \\ \boldsymbol{T}e^{bl}\cos(2\pi l) + P^*(t), & \boldsymbol{p} < 0.5 \cap |\boldsymbol{Q}| \geq 1 \\ \boldsymbol{P}_{\text{rand}} - \boldsymbol{QT}, & p \geq 0.5 \end{cases} \\ \boldsymbol{T} &= |\boldsymbol{P}^*(\boldsymbol{t}) - \boldsymbol{P}(\boldsymbol{t})| \end{aligned} \tag{13}$$

where t is the iteration index, $\boldsymbol{P}(\boldsymbol{t})$ represents the current position vector, $\boldsymbol{P}^*(\boldsymbol{t})$ denotes the current global optimal solution, $\boldsymbol{P}_{\text{rand}}$ is the current random position vector, p is a stochastic probability, when $p \geqslant 0.5$, random search is executed. $\boldsymbol{Q}$ is the coefficient vector, under $p < 0.5 \cap |\boldsymbol{Q}| < 1$ indicates encircling prey behavior, otherwise signifies spiral movement, $\boldsymbol{T}$ represents the distance to the optimal solution, b is the spiral constant controlling tightness, fixed at $b = 1$, l represents the spiral path parameter, $l \in [-1,1]$.

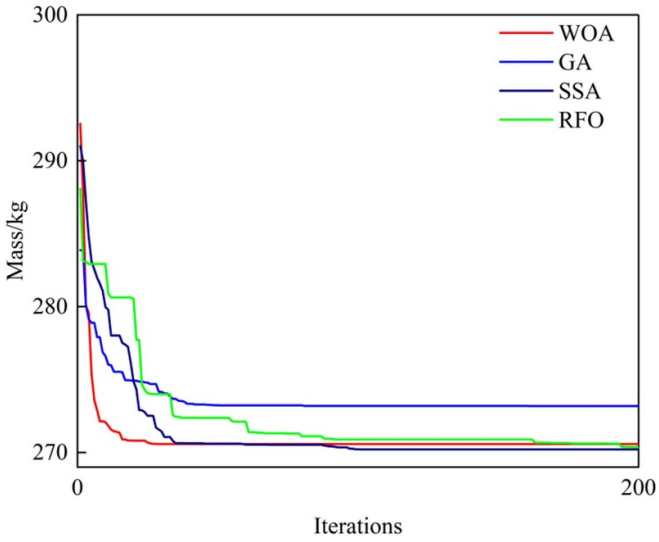


Figure 6. Convergence performance of metaheuristic algorithms in RBDO.

5. Case study analysis

This case study focuses on a dual rotary table, where the core load-bearing structures (cradle frame and worktable) are manufactured from HT300 gray cast iron using an integral casting process.

5.1. Analysis of topology optimization results

According to technical manuals and FEA, the system experiences maximum deformation (0.017 517 mm) under rated maximum load with 21° A-axis rotation of the cradle frame. The peak deformation occurs along the negative Y-direction at 0.014 582 mm. This operating condition defines the limit state for RBDO, while serving as the critical design scenario for topology optimization. Mechanical analysis of the optimized base structure identifies stress concentration zones at contact boundaries between the cradle frame periphery and C-axis core tube. Subsequently, compliance-minimization topology optimization generates compliant stiffening ribs, symmetrically arranged around bilateral main beams. This configuration suppresses interference at contact boundaries while fulfilling structural performance requirements.

5.2. Building of parametric models

To implement RBDO, this study refers to the final topology optimization results from the previous section to construct a parametric model. The parameter extraction process comprises four sequential steps: firstly, tracking material distribution evolution during optimization to extract ten initial dimensional parameters (D_1–D_{10}) (figure 7(a)). Secondly, performing Sobol sensitivity analysis of these parameters for their effects on dual rotary table mass and deformation (figure 7(b)). Thirdly, eliminating dimensional parameters D_9 and D_{10} that exhibit low sensitivity to both responses. Finally, defining manufacturability and assembly constraints for the retained dimensional parameters D_1–D_8, with detailed boundary specifications provided in table 1.

5.3. Optimization function

This study minimizes system mass as the primary objective, incorporating stochastic uncertainties through chance constraints. The mathematical formulations of the optimization problem are as follows.

First, due to assembly constraints, the side stiffening ribs must not extend beyond the highest points at both ends of the cradle frame. This constraint is mathematically defined as $G_1(\boldsymbol{X})$:

$$G_1(\boldsymbol{X}) = D_2 \tan D_1 - 306. \tag{14}$$

Second, in the solution space, the system deformation under limit-state conditions must not exceed $L_{\max}$, defined by the constraint function $G_2(\boldsymbol{X})$:

$$G_2(\boldsymbol{X}) = L_{\max} - L(\boldsymbol{X}) \tag{15}$$

where $L_{\max}$ represents the maximum value of system deformation, equal to 0.017 432 mm.

Considering the specificity of the dual rotary table, the optimization results must simultaneously satisfy a reliability requirement greater than 99%, defined by the constraint function $R(\boldsymbol{X})$:

$$R(\boldsymbol{X}) = R_i - 0.99. \tag{16}$$

Transforming the constraint set and dimensional bounds into a penalty function effectively reduces constraint violations during the solution process [40, 41]. In essence, the penalty factor functions as a weighting coefficient, the magnitude of which correlates with the relative importance of each constraint within the optimization problem. This approach

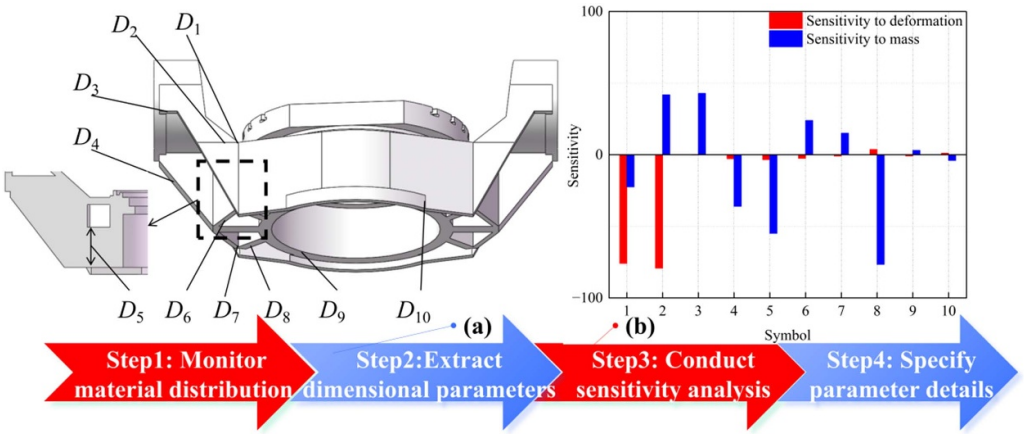


Figure 7. Topology-to-parameter translation workflow.

Table 1. Specifications of dimensional parameters.

Symbol	Initial Value	Bounds	Distribution	COV
D_1/°	45	[42,60]	Normal	0.02
D_2/mm	95	[60,105]	Normal	0.02
D_3/mm	52	[5,95]	Normal	0.02
D_4/mm	30	[10,160]	Normal	0.02
D_5/mm	100	[50,150]	Normal	0.02
D_6/mm	10	[5,50]	Normal	0.02
D_7/mm	15	[5,50]	Normal	0.02
D_8/°	60	[50,90]	Normal	0.02

yields the final objective function for the proposed optimization framework:

$$\min M(\boldsymbol{X}) = M(\boldsymbol{X}) + \sum_{i=1}^{2} [p_g |G_i(\boldsymbol{X})|] + p_r |R(\boldsymbol{X})| \quad (17)$$

where p_g weights stiffness violations in $G_i(\boldsymbol{X}) \leqslant 0$, fixed at $p_g = 0.5$, p_r penalizes reliability constraint violations in $R(\boldsymbol{X}) \leqslant 0$, fixed at $p_r = 0.5$.

5.4. Validation of the AK surrogate model fitting

This study employs AK-MCS to overcome computational bottlenecks in RBDO. FEA was conducted via ANSYS Mechanical (v2023 R1) on a Lenovo laptop with Intel i7-1065G7 (4 cores @ 1.5GHz) and 16 GB RAM. Under this configuration, the crude Monte Carlo method requires 1833 h of FEA computation, while AK-MCS generates equivalent predictions in only 7.4 s, achieving substantial computational savings. Latin hypercube sampling was implemented to randomly generate 90 sets of dimensional parameters as design variables, with system mass and deformation as responses.

To validate the AK-MCS model, 10 samples were selected from this sample set as a verification set. As shown in figure 8, all verification points exhibit relative errors below 1%, confirming the model's high predictive accuracy.

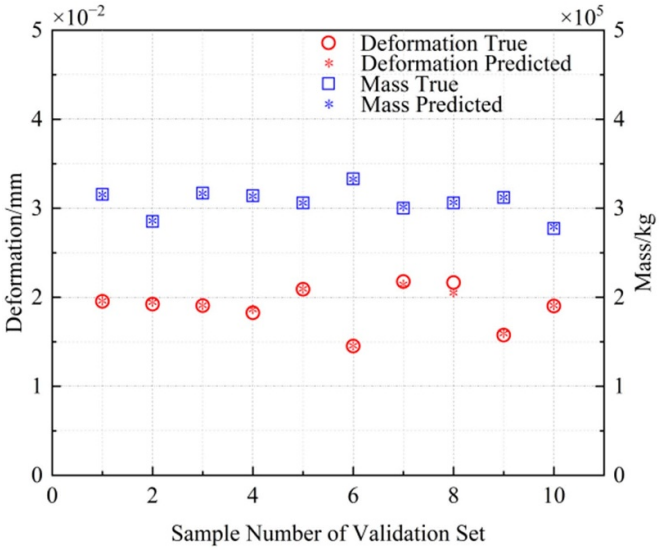


Figure 8. Validation of predicted deformation and mass for samples.

5.5. Results and discussion

This study embedded the AKS model within WOA to solve the optimization problem. Ten independent repeated experiments were conducted, with iterative convergence profiles shown in figure 9. All trials converged within 200 iterations, justifying the maximum iteration count of 200 for WOA.

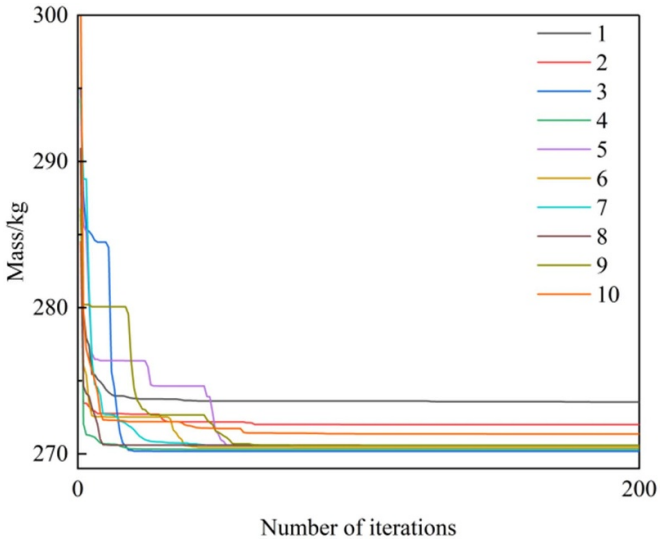


Figure 9. Convergence analysis of WOA.

Table 2. Comparison of optimized dimensional parameters.

Symbol	DDO	RBDO
D_1/°	42	42
D_2/mm	81.343	87.517
D_3/mm	95	94.999
D_4/mm	10	10.016
D_5/mm	50	76.753
D_6/mm	5	5
D_7/mm	5	5
D_8/°	70.616	78.767
Cradle frame mass/kg	269.965	270.945
Deformation/mm	0.017 432	0.016 839
Reliability	66.11%	99.47%

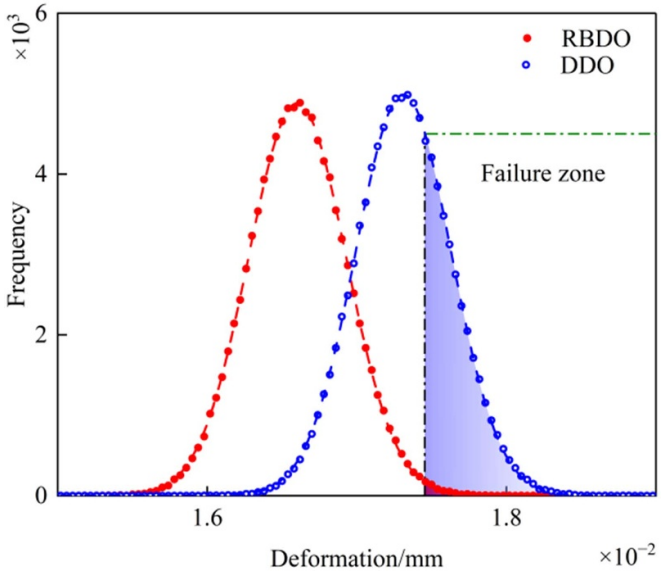


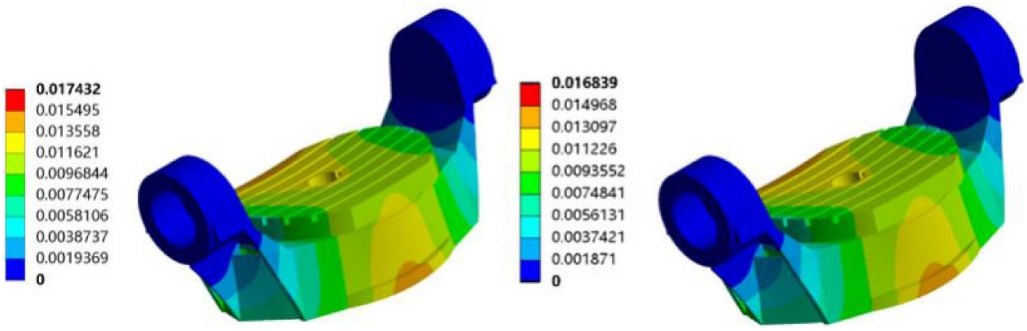
Figure 10. Comparison of probability density distributions.

Algorithmic parameters, including a population size of 150 search agents, were initialized according to [37–39], with calibration adjustments (figure 9) addressing potential issues in RBDO implementation. To ensure solution accuracy, the finite element method performed cross-validation on two optimized parameter sets, achieving a mean error of 0.46%, thereby confirming result reliability. Specific dimensional parameters and performance comparisons are detailed in table 2.

As critical components of machine tools, dual rotary tables demand high structural reliability [42]. DDO approach achieved 66.11% reliability, but insufficient for the required reliability exceeding 99%. By integrating reliability constraints into DDO, this study increased mass by merely 0.36% while substantially improving reliability from 66.11% to 99.47%, as illustrated in figure 10. Under limit-state conditions, RBDO framework yielded a deformation of 0.016839 mm with a 51.05% mass reduction compared to the initial 530 kg pre-optimization mass (resulting mass: 270.542 kg). Under identical driving torque, reduced system inertia enables rotational speeds reaching 104.28% of baseline values. Concurrently, this design reduces inertial loads on braking mechanisms, enhancing positioning accuracy and dynamic performance.

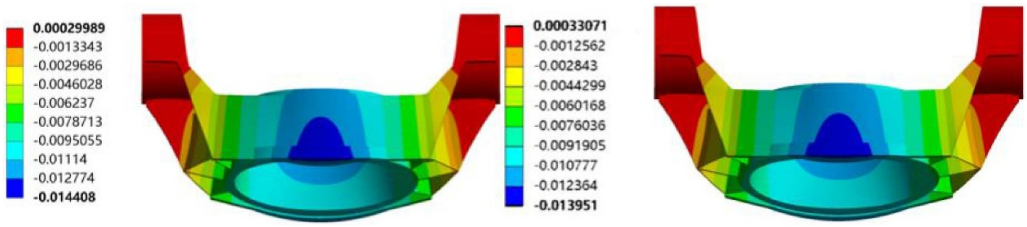
5.6. Verification of optimization results

Finally, the AKS model obtained through WOA iterative computation was subjected to FEA. The prediction error of the optimization algorithm was only 0.46%, well below the upper error limit of 1%. The FEA results for both DDO and RBDO are shown in figures 11 and 12. RBDO not only improved the reliability of the dual rotary table but also reduced the deformation. Compared to DDO, RBDO reduced the maximum deformation by 3.4%, with the maximum axial deformation still occurring in the negative Y-axis direction—showing a 3.17% reduction in deformation under RBDO. Furthermore, the FEA results further validate the significant enhancement



(a) DDO (b) RBDO

Figure 11. Comparison of total deformation of the system.



(a) DDO (b) RBDO

Figure 12. Comparison of the Y-axis deformation amount of the system.

in stiffness provided by the stiffening ribs to the dual rotary table. Compared to the non-ribbed structure obtained from global topology optimization (as shown in figure 4(c)), RBDO reduced deformation by 10.6%. In summary, the dual rotary table structure designed and optimized in this study achieves high reliability while maintaining an optimal balance between mass and stiffness, making it a high-performance component for CNC machine tools.

6. Conclusions

This study presents a holistic design optimization methodology for dual rotary tables in five-axis CNC machine tools, covering the entire process from initial conceptual design to a finalized configuration. The approach significantly reduces the impact of subjective human factors during the early design stage and ultimately yields a high-performance dual rotary table. The major contributions and findings are summarized as follows:

(1) A two-stage topology optimization process was implemented. Global topology optimization aimed at mass reduction, while local topology optimization successfully incorporated stiffening ribs in stress concentration zones. This resulted in a dual rotary table structure that achieves an optimal balance between mass and stiffness.
(2) Eight key dimensions sensitive to both deformation and mass were extracted from the topology-optimized structure. WOA was effectively integrated with the AK-MCS method for optimization, leading to the development of an AKS model with a prediction error of only 0.46%.
(3) Compared to the DDO approach, RBDO design improved structural reliability from 66.11% to 99.47%, reduced deformation by 3.4%, and increased mass by a mere 0.36%. Compared to the initial pre-optimization mass of 530 kg, the final mass was reduced by 51.05% to 270.542 kg. This substantial mass reduction significantly decreases the load on the braking mechanism, thereby enhancing the machining accuracy and robustness of the five-axis machine tool.

It should be noted that to ensure manufacturability, the values of the design parameters were constrained within conservative ranges. Future research will focus on exploring the manufacturability limits of complex topologically optimized structures to establish more precise and practical design windows for production-oriented optimization.

Data availability statement

The data cannot be made publicly available upon publication because they are not available in a format that is sufficiently accessible or reusable by other researchers. The data that support the findings of this study are available upon reasonable request from the authors.

Conflict of interest

The authors declare no conflict of interest.

On behalf of all authors, the corresponding author states that there is no conflict of interest.

Authors contributions

Dongheng Li: Conceptualization, Methodology, Software, Writing-original draft. Mingfei Ma: Writing-reviewing. Xianzhen Huang: Supervision and correction, Funding acquisition. Yuping Wang: Technical instruct. Zhiyuan Lu: Data analysis. Peilong Li: Validation and Editing.

Funding

This research is financially supported by the National Natural Science Foundation of China (U23B2098, U22B2087), the Applied Basic Research Program of Liaoning Province (2023JH2/101300160) and the Fundamental Research Funds for the Central Universities (N2403002).

ORCID iDs

Dongheng Li 0009-0008-2583-8009
Xianzhen Huang 0000-0003-1924-3515
Yuping Wang 0000-0002-7805-3773

References

[1] Zhang Z, Jiang F, Luo M, Wu B H, Zhang D H and Tang K 2024 Geometric error measuring, modeling, and compensation for CNC machine tools: a review *Chin. J. Aeronaut.* **37** 163–98
[2] Soori M and Asmael M 2023 Minimization of deflection error in five axis milling of impeller blades *Facta Univ. Ser.: Mech. Eng.* **21** 175–90
[3] Chu C-H, Zhou Y S, Liu E-M and Tang J Y 2022 Optimal tool path generation and cutter geometry design for five-axis CNC flank milling of spiral bevel gears *J. Comput. Des. Eng.* **9** 2024–39
[4] Makhanov S S 2022 Vector fields for five-axis machining. A survey *Int. J. Adv. Manuf. Technol.* **122** 533–75
[5] Sun S J, Zhao P, Zhang T, Li B B and Yu D 2024 Smoothing interpolation of five-axis tool path with less feedrate fluctuation and higher computation efficiency *J. Manuf. Process.* **109** 669–93
[6] Chen L J, Tang J M, Wu W Y and Wei Z S 2023 Nonlinear error compensation based on the optimization of swing cutter trajectory for five-axis machining *Int. J. Adv. Manuf. Technol.* **124** 4193–208
[7] Guo Z W, Zhang S, Shi J and Sun J H 2025 A modified method for measuring geometric errors of rotary axes based on sensitivity analysis and error simulation *Measurement* **242** 115968
[8] Chen Y-T, Liu C-S and Yan Y-J 2025 Synchronous measurement and verification of the position-independent geometric errors of dual rotary axes on five-axis machine tools *Int. J. Precis. Eng. Manuf.* **26** 1411–29
[9] Cui R, Ma M F, Liu H Q, Tan Z, Huang X Z and Zhang Y M 2024 Tolerance analysis of cradle-type double rotary table using the local parallel dimension chain method *Int. J. Adv. Manuf. Technol.* **134** 5679–96
[10] Tang Z W, Zhou Y S, Wang S H, Zhu J and Tang J Y 2022 An innovative geometric error compensation of the multi-axis CNC machine tools with non-rotary cutters to the accurate worm grinding of spur face gears *Mech. Mach. Theory* **169** 104664
[11] Cui Y Z, Liu C X, Mu H J, Jiang H, Xu F X, Liu Y F and Hu Q M 2024 Analysis of mechanical characteristics of the swing angle milling head of a heavy computer numerical control milling machine and research on the light weight of a gimbal *Materials* **17** 324
[12] Li J K, Hu K F, Zhang X, Qian Y B, Zhao J and Feng Q B 2025 Method for simultaneously measuring four-degree-of-freedom geometric errors of a rotary axis based on circular grating *Opt. Express* **33** 10649–59
[13] Hao P, Wang Y, Jin L Z, Ma S H and Wang B 2023 An isogeometric design-analysis-optimization workflow of stiffened thin-walled structures via multilevel NURBS-based free-form deformations (MNFFD) *Comput. Methods Appl. Mech. Eng.* **408** 115936
[14] Meng Z, Luo X H and Zhou H L 2022 Lightweight design of arcuately stiffened cylindrical shells based on smeared stiffener method and active learning strategy *Thin-Walled Struct.* **174** 109167
[15] Pham H-A, Tran H-Q, Tran M-T, Nguyen V-L and Huong Q-T 2022 Free vibration analysis and optimization of doubly-curved stiffened sandwich shells with functionally graded skins and auxetic honeycomb core layer *Thin-Walled Struct.* **179** 109571
[16] Jiang X D, Liu C, Du Z L, Huo W D, Zhang X Y, Liu F and Guo X 2022 A unified framework for explicit layout/topology optimization of thin-walled structures based on Moving Morphable Components (MMC) method and adaptive ground structure approach *Comput. Methods Appl. Mech. Eng.* **396** 115047
[17] Li Y, Gao T, Zhou Q Y, Chen P, Yin D Z and Zhang W H 2023 Layout design of thin-walled structures with lattices and stiffeners using multi-material topology optimization *Chin. J. Aeronaut.* **36** 496–509
[18] Yoshimura M and Izui K 2002 Smart optimization of machine systems using hierarchical genotype representations *J. Mech. Des.* **124** 375–84
[19] Cui M T, Cui W N, Li W and Wang X B 2024 A polygonal topology optimization method based on the alternating active-phase algorithm *Electron. Res. Arch.* **32** 1191–226
[20] Liu H Y, Qiu Z, Shi J, Sun J H and Zhang S 2025 Ground structure method-based stiffener layout topology optimization for horizontal machining center headstock cover plate *Comput. Struct.* **307** 107633
[21] Veluswamy A, Venugopal P R, Mani K, Palanisamy D, Marikrishnan T and Arunachalam A T 2024 Topology optimization-based design, development and testing of steel-reinforced epoxy granite vertical machining centre column *Proc. Inst. Mech. Eng. L* **238** 1005–20
[22] Hao Y P, Zhu L D, Yan B L, Ren T Y, Zhao J Z, Ning X F and Lu H 2023 Stiffness design and multi-objective optimization of machine tool structure based on biological inspiration *J. Vib. Control* **29** 2774–88
[23] Audibert C, Chaves-Jacob J, Linares J-M and Lopez Q-A 2018 Bio-inspired method based on bone architecture to optimize the structure of mechanical workpieces *Mater. Des.* **160** 708–17
[24] Yeh T P and Vance J M 1998 Applying virtual reality techniques to sensitivity-based structural shape design *J. Mech. Des.* **120** 612–9
[25] Shan W C, Ding Y and Zhou J W 2022 Automatic structural optimization design using sensitivity-based method *Structures* **46** 99–108
[26] Ma M F, Liu H Q, Wu X J, Tan Z, Huang X Z and Zhang Y M 2025 Global reliability sensitivity analysis of cradle-type double rotary table *Proc. Inst. Mech. Eng. C* **239** 1492–505
[27] Meng Z, Guo L B and Wang X 2022 A general fidelity transformation framework for reliability-based design

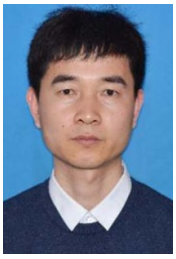
optimization with arbitrary precision *Struct. Multidiscip. Optim.* **65** 14
[28] Lu L, Wu Y Z, Zhang Q and Qiao P A 2023 Transformation-based improved Kriging method for the black box. Problem in reliability-based design optimization mathematics *Mathematics* **11** 218
[29] Meng Z, Yildiz A R and Mirjalili S 2022 Efficient decoupling-assisted evolutionary/metaheuristic framework for expensive reliability-based design optimization problems *Expert Syst. Appl.* **205** 117640
[30] Jiang Z Y, Huang X Z, Ding P F, Liu H Z and Ge Y 2023 Reliability-based design optimization of the spiral water jacket for motorized spindle *Case Stud. Therm. Eng.* **51** 103665
[31] Benzley S E, Perry E, Clark B and Sjaardama G 1995 A comparison of all hexagonal and all tetrahedral finite element meshes for elastic and elasto-plastic analysis *Proc. 4th Int. Meshing Roundtable. Albuguergue: Sandia National Laboratories* pp 179–91
[32] Sigmund O and Petersson J 1998 Numerical instabilities in topology optimization: a survey on procedures dealing with checkerboards, mesh-dependencies and local minima *Struct. Multidiscip. Optim.* **16** 68–75
[33] Jiang C, Qiu H B, Gao L, Wang D P, Yang Z and Chen L M 2020 Real-time estimation error- guided active learning Kriging method for time-dependent reliability analysis *Appl. Math. Modelling* **77** 82–98
[34] Wang X, Jiang Z Y, Huang X Z, Sun L S and Wang Y P 2025 Surface topography prediction and reliability analysis of ball end milling *Measurement* **242** 115770
[35] Ma M F, Huang X Z, Liu H Q, Wu X J, Hua C L and Zhang Y M 2025 Reliability-based design optimization of a cradle-type double rotary table for 5-axis machining center *Mech. Based Des. Struct. Mach.* 1–25
[36] Echard B, Gayton N and Lemaire M 2011 AK- MCS: an active learning reliability method combining Kriging and Monte Carlo simulation *Struct. Saf.* **33** 145–54
[37] Mirjalili S and Lewis A 2016 The whale optimization algorithm *Adv. Eng. Softw.* **95** 51–67
[38] Nadimi-Shahraki M H, Zamani H, Varzaneh Z and Mirjalili S 2023 A systematic review of the whale optimization algorithm: theoretical foundation, improvements, and hybridizations *Arch. Comput. Methods Eng.* **30** 4113–59
[39] Osama A *et al* 2023 Optimal placement and sizing of capacitor banks in radial distribution systems using the whale optimization algorithm *2023 IEEE PES Conf. on Innovative Smart Grid Technologies, ISGT Middle East*
[40] Jafari-Asl J, Ben Seghier M E A, Ohadi S and van Gelder P 2021 Efficient method using whale optimization algorithm for reliability- based design optimization of labyrinth spillway *Appl. Soft Comput.* **101** 107036
[41] Wang Y P, Chang M X, Huang X Z, Li Y X and Tang J W 2023 Cutting tool wear prediction based on the multi -stage Wiener process *Int. J. Adv. Manuf. Technol.* **129** 5319–33
[42] Wang H, Zhang Y M, Yang Z and Wang W 2018 Investigation on the multifactor reliability allocation method for CNC lathes based on modified criticality and objective *Proc. Inst. Mech. Eng. C* **232** 1647–56



Dongheng Li received the BE degree in Mechanical Engineering, from Northeastern University, China, in 2024, where he is currently pursuing an academic master's degree. His current research interests include topology optimization and machine tool reliability.



Mingfei Ma is a PhD candidate at Northeastern University, with research focusing on machine tool dynamics and reliability.



Professor Xianzhen Huang is a PhD Supervisor at the School of Mechanical Engineering and Automation, Northeastern University. His research primarily focuses on mechanical reliability, industrial big data, and robot mechanisms.



Yuping Wang received the BE degree in mechanical design, manufacturing and automation from Taiyuan University of Technology, China, in 2021, and the MS degree from the School of Mechanical Engineering and Automation, Northeastern University, China, in 2024, where he is currently pursuing the PhD degree. His current research interests include prognostics and health management, stochastic process, and structure reliability.



Zhiyuan Lu is a Master's student in Mechanical Engineering, Northeastern University.



Peilong Li is currently studying at Northeastern University and mainly engaged in research on five-axis milling forces and its reliability.